Original Research Article

Magnetic Characterization of Co and Zn Nano Ferrites: Property Consideration for Oil-Spill Clean up

ABSTRACT

Aim: This work studied the magnetic properties of Co and Zn nano-ferrites, $CoFe_2O_4$ and $ZnFe_2O_4$ respectively, with considerations for the properties that are desirable for oil spill cleanup.

Study design: Experimental

Place and Duration of Study: Department of Physics, Faculty of Physical Sciences, Bayero University Kano, Nigeria and department of Physics, Federal University Dutse, Jigawa State, Nigeria between July 2020 and October 2021.

Methodology: The ferrite nanoparticles were synthesized by the glycol-thermal method at 200 ºC for 6 hours using a stirred pressure reactor.

Results: Single phase spinel crystal structures were obtained for both samples as determined by an X-ray diffraction (XRD) machine. The high-resolution transmission electron microscope and surface electron microscope images showed nano structures. The magnetic properties and magnetic hyperfine parameters were determined using a lakeshore vibrating sample magnetometer and ^{57}Fe Mössbauer spectroscopy. The XRD peaks were consistent with that of a single phase spinel structure. No impurity phase was detected. The nano-ferrites have crystallite sizes of about 10 nm and 17 nm for $CoFe_2O_4$ and $ZnFe_2O_4$. The nano almost-spherical nature of the samples was also confirmed from their morphology studies Single phase spinel crystal structures were obtained for both samples as determined by an X-ray diffraction (XRD) machine. The high-resolution transmission electron microscope and surface electron microscope images showed nano structures. The magnetic properties and magnetic hyperfine parameters were determined using a lakeshore vibrating sample magnetometer and ^{57}Fe Mössbauer spectroscopy. The XRD peaks were consistent with that of a single phase spinel structure. No impurity phase was detected. The nano-ferrites have crystallite sizes of about 10 nm and 17 nm for $CoFe_2O_4$ and $ZnFe_2O_4$. The nano almost-spherical nature of the samples was also confirmed from their morphology studies.

Conclusion: The saturation magnetization of $CoFe_2O_4$ and $ZnFe_2O_4$ were about 50 emu/g and 30 emu/g respectively. They both exhibited superparamagnetic properties with a component of para-magnetism observed in $ZnFe_2O_4$ nano-ferrites. $CoFe_2O_4$nano-ferrites exhibited better desired property for oil spill cleanup. The $ZnFe_2O_4$ nano-ferrites showed tendencies of slow response to magnetic field, however, it is more environmentally friendly. The magnetic hyperfine parameters and the isomer shift values for $CoFe_2O_4$ and $ZnFe_2O_4$ showed strong internal magnetic fields and the obtained values are consistent with spinel structure. The oxidation state of Fe was observed to be Fe^{3+}. Due to the low coercivity and

high magnetization values, these particles could be considered as potential; candidates for oil spill cleanup. These desirable magnetic properties will improve the recyclability of the nanoparticles using low applied magnetic fields.

Keywords: Glycol-Thermal, Single Phase Spinel, Superparamagnetic, Coercivity, ^{57}Fe Mössbauer Spectroscopy

1.0 INTRODUCTION

The emergence of nanotechnology has revolutionized innovations in almost all fields of endeavors such as in agriculture, pharmaceuticals, medicals, electronics, energy, environmental management, the oil and gas industry, aerospace and automobile [1]. It is an interdisciplinary technology that involves the application of materials with a size range of about 1-100 nm, known as nanomaterials [2]. The unique properties derived from nanomaterials found interesting applications compared to their bulk counterpart. This is primarily due to the nano-size effect which gives nanomaterials a high surface to volume ratio, increased number of surface atoms and enhanced reactivity [3]. Magnetic, optical, and electrical properties at the nano-scale behave very differently from the bulk samples. The understanding of these properties has enabled the deployment of nanotechnology in the oil and gas industries in areas such as exploration, drilling, logging, hydraulic fracturing, formation damage, enhanced oil recovery (EOR) and ex-situ upgrading of oil shales/bitumen [2-5]. A more recent possible application of nanomaterials for environmental remediation is found in the oil and gas sector, which involves the use of amine functionalized or polymer coated magnetic nanoparticles for cleaning crude oil spills [3]. Therefore, there are enormous potentials in understanding the behavior of materials at nano-scale so that the properties can be tailored towards specific application.

The cubic spinel ferrites are one of such materials that are suitable for environmental remediation application. Ferrites belong to a special class of ceramic oxides with a general chemical formula of AB_2O_4, where *A* represents one or a mixture of the divalent transition metals such as, zinc (Zn), iron (Fe), magnesium (Mg), nickel (Ni), cobalt (Co), copper (Cu), or calcium (Ca) [6], and *B* represents solely iron (Fe). Generally, a cubic spinel structure consists of two interstitial sites known as tetrahedral *A* and octahedral *B* ions which contains 8 tetrahedral coordinated sites and 16 octahedral coordinated sites for divalent & trivalent metal cation occupancy, where *A* and *B* denote divalent and trivalent cations respectively [7-8]. For an ideal normal spinel of $ZnFe_2O_4$ ferrites, Zn^{2+} exclusively occupies the tetrahedral *A*-sites while Fe^{3+} occupies the octahedral *B*-sites. A mixed cation

UNDER PEER REVIEW

distribution is the case for $MgFe_2O_4$. Such distributions of cations significantly influence the magnetic properties of the ferrites [9].

A generic example is $C_xD_{1-x}Fe_2O_4$ where, $0 \leq x \leq 1$. At both extreme conditions for x = 0 or x = 1, DFe_2O_4 or CFe_2O_4 ferrites are obtained respectively. However, an intermediate case is obtained for x = 0.5 as is the case for $C_{0.5}D_{0.5}Fe_2O_4$ ferrite. Consequently, one could vary the structural and magnetic properties of the ferrite by establishing different intermediate cases. Also, the method of synthesis could also have effect on the magnetic properties of nanoparticles [10].

The current project synthesized single phase nanoparticles of $CoFe_2O_4$ and $ZnFe_2O_4$ ferrites using the glycol-thermal synthesis method. The selected elements such as Fe and Zn are environmentally friendly. However, Zn has low anisotropy compared to Co. Therefore, Co is selected because of its high anisotropy so as to improve the magnetization of the sample and help in making comparison.

2. THEORETICAL BACKGRAOUND

High saturation magnetization M_S and low coercivity H_C are characteristic features of superparamagnetic materials. The magnetization measures the magnetic spins response to magnetic field. The response is produced in a loop called the magnetic hysteresis loop. It is the magnetic spin response to the application and removal of magnetic field. Figure 2.4 shows a schematic diagram of the magnetic hysteresis loop responses from materials with the different main classes of magnetic order in solids.

The M_S can be empirically calculated from the law of approach to saturation magnetization given by [11]:

$$M(H) = M_S\left(1 - \frac{a}{H} - \frac{b}{H^2}\right) + \chi H \quad , \tag{1}$$

where a and b are constants, M_S is the saturation magnetization and χ_{hf} is the high field susceptibility. The a/H term is attributed to structural defects or nonmagnetic inclusions. The b/H^2 term is due to uniform magneto-crystalline anisotropy.

The coercivity gives a measure of the anisotropy of a magnetic material [12]. This can be estimated by:

UNDER PEER REVIEW

$$H_C = \frac{|H_{C1}| + |H_{C2}|}{2}, \quad (2)$$

where H_{C1} and H_{C2} are the negative and positive coercivity respectively along the magnetic field direction [13]. Soft superparamagnetic materials are expected to have insignificant or almost zero coercivity thereby quenching the propensity for high degree of agglomeration of the nanoparticles and the demand for high magnetic field. This implies that it will be easier to recycle the magnetic nanoparticles after every cycle of magnetization for reuse in the oil spoil cleaning process.

Micro-structural properties such as crystallite size D and lattice parameters a could significantly contribute to changes in structural and magnetic properties of materials [14-15-16]. The Debye–Scherrer formula;

$$D = \frac{K\lambda}{W_{(hkl)}\mathrm{Cos}\,\theta}, \quad (3)$$

It is often used Equation (3) to estimate D, where K is a constant associated with the shape factor with a value of about 0.94 for a spherical shape, λ is the X-ray diffraction wavelength, W is the full width at half maximum, θ is the Bragg's angle and hkl are the Miller indices of a selected intensity peak [17].

Also, from Bragg's law of diffraction, one could establish that the lattice parameters *a* for a cubic crystal structure has a relationship with hkl as;

$$a = \frac{\lambda}{2\mathrm{Sin}\,\theta}\sqrt{h^2 + k^2 + l^2}\,. \quad (4)$$

3. MATERIAL AND METHODS

The materials and methodology are presented for the research work.

2.1Glycol-Thermal Synthesis Method

The glycol-thermal synthesis method is a wet chemical method that involves the use of stoichiometric precursors of metal chlorides or nitrates that are dissolved in de-ionized water to form a mixed solution of starting compounds. Ammonia, potassium hydroxide or sodium hydroxide can be used to precipitate the metal chlorides or nitrates from solutions.

UNDER PEER REVIEW

This is performed while continuously stirring the solution until a deserved pH of about 9 is reached. The precipitate is then washed several times in de-ionized water to get rid of the chlorides or nitrates. This is followed by the reaction of the precipitate in ethylene glycol in a high pressure reactor. A PARR 4843 stirred pressure reactor was used for the synthesis of the materials. The reaction chamber houses a stirrer that enables the continuous stirring of the reactants during synthesis. The reaction conditions such as stirring speed, pressure and temperature are recorded.

The $CoFe_2O_4$ and $ZnFe_2O_4$nano-ferrites used in the present work were synthesized by the glycol-thermal method. The nano ferrites were synthesized from $FeCl_3.6H_2O$ (99%), $CoCl_2.6H_2O$ (98%) and $ZnCl_2.6H_2O$ (98%). All chemicals were used as purchased from Sigma-Aldrich Chemicals. The stoichiometric chlorides were initially dissolved in 400 ml of de-ionized water in a beaker placed on a magnetic stirrer at different times for the synthesis of $CoFe_2O_4$ and $ZnFe_2O_4$nano-ferrites. A pH value of 2.51 was initially recorded. After 20 minutes of continuous stirring for the homogeneous mixture, ammonium solution was gradually added to initiate precipitation of the metal chlorides until a pH of 9 which was maintained for 30 minutes while stirring. The precipitated solution was washed several times over a Whatman (GF/F 110 mm) glass microfibre filter in a Büchner funnel with de-ionized water in order to get rid of chlorides. The absence of chlorides was confirmed by the addition of standard solution of $AgNO_3$ to the filtrate until no precipitate of $AgCl_2$ was detectable. The washed precipitate was recovered from the filter, mixed with 250 ml of ethylene glycol and transferred into the reaction chamber. The reactor was operated at a soak temperature of 200 ºC for 6 hours at a stirring speed and pressure of 300 rpm and 80 psi respectively. The cooled final product was finally filtered over a fresh Whatman filter and rinsed with 200 ml of ethanol. The sample was allowed to dry on the filter paper under a 200 W infrared light for 24 hours. The dried blackish sample was homogenized into fine powder by agate mortar and pestle, and stored for characterizations.

UNDER PEER REVIEW

2.2 Sample Characterization

2.2.1 X-ray Diffraction

X-ray diffraction (XRD) is a structural characterization technique for the identification of the crystalline structure and identification of different phases in a sample. Information about the spacing between rows of atoms known as the *d* spacing can be derived. XRD data also provides the possibility of measuring the size, shape and internal stress of small crystalline regions and the orientation of a single crystal [18]. The technique operates on the

principle of diffraction where the atomic planes of a crystal cause incident beams of X-rays to interfere with each other as they leave the crystal. Diffraction occurs only when Bragg's law is satisfied. Mathematically Bragg's law is expressed as;

$$n\lambda = 2d\sin\theta, \tag{5}$$

where n is an integer, λ is the wavelength of the incident beam and θ is the angle between the incident beam and the scattering plane. The lattice constant a of a cubic crystal has a relationship with the d spacing of a sample by the following equation;

$$a = d\sqrt{h^2 + k^2 + l^2}\,. \tag{6}$$

Therefore, substituting Bragg's law into the Equation (6) gives Equation (4). It is from the XRD high intensity peak (311) that the crystallite size of the nanoparticles is estimated using Equation (3).

3.2.2 High Resolution Transmission and Scanning Electron Microscopy

High resolution transmission electron microscopy (HRTEM) is an imaging technique that is used to perform size, shape and crystallographic structure analysis of samples in the micro, nano and sub-nanometer range. The basic principle of operation is such that images formed are generated from the interaction of electron beams transmitted through a thin sample. The images are usually magnified and focused by an objective lens and appear on an imaging screen detected by a sensor such as charge-coupled device camera. Sample preparation for HRTEM is crucial as the images can be affected by the thickness of the sample. A Joel-JEM-2100 high resolution transmission electron microscope was used to study the samples in the current work. A small sample size of about 0.0001 g was dispersed in ethanol and vibrated in an 80Hz\40Watt transistorized sonic cleaner for 3 minutes. A copper thin film sample holder with diameter of about 0.0005 mm is dipped into the dispersed sample and loaded in the equipment in order to produce scanned images of the sample.

High resolution scanning electron microscopy (HRSEM) is a technique that explores the surface morphology of a sample. The principle of its operation is similar to that of the HRTEM except that the electron beam is directed mainly at the surface of a sample. Signals are generated when the beam of electrons strikes the surface of a sample. This provides some energy level information about the elemental composition of the sample. The technique is also referred to as energy dispersive X-ray. A Zeiss ultra plus high resolution scanning electron microscope was used to perform measurements in this work. In order to

UNDER PEER REVIEW

prepare sample for scanning, one side of a carbon tape with two-sided sticky surfaces is secured on the sample holder. The other surface is then lightly matched over the sample and wiped lightly with a filter paper to avoid particles dropping off or too much sample on the surface. To avoid charging of the sample by the electron beam, the sample is usually coated with gold using a Polaron SC 500 sputter coater.

2.2.3 Magnetization Measurements

The magnetization measurements were obtained using a LakeShore model 735 vibrating sample magnetometer (VSM). The sample rod was mounted into a Janis model helium cryostat and only a maximum applied magnetic field of about 14 kOe was available for this system. The system consists of a 735 VSM controller and the vibrating head which is mounted above the Janis helium cryostat. The bottom neck of the cryostat is centered between the pole faces of the electromagnet. Pick-up coils are mounted on the faces of the poles of the electromagnet. Other critical components of the system include a 642 bipolar electromagnet power supply, 340 temperature controller, 450 Gaussmeter, a NESLAB ThermoFlex 2500 chiller and a National Instrument IEEE-488 interface card installed in a desktop computer for data collection.

The principle of operation of a VSM is based on Faraday's law of induction which defines the induced voltage produced in the pick-up coils that is proportional to the magnetization of the sample. In Faraday's law;

$$\frac{d\Theta}{dt} = -E, \tag{7}$$

where $\frac{d\Theta}{dt}$ is the rate of change of magnetic flux and *E* is the induced voltage. The technique measures the magnetic moment by detecting the AC field produced by the oscillation of a magnetized sample. The magnetization of the sample is proportional to the amplitude of the induced signal. The VSM was calibrated using a standard nickel sphere. The sample to be measured is placed in a cylindrical sample holder which is screwed to the lower end of the vibrating sample rod. The rod is gently lowered into the sample space to the final position of the sample between the pick-up coils. The data is collected using the interface card and the data acquisition software installed on the computer.

UNDER PEER REVIEW

2.2.4 ^{57}Fe Mössbauer setup and measurements

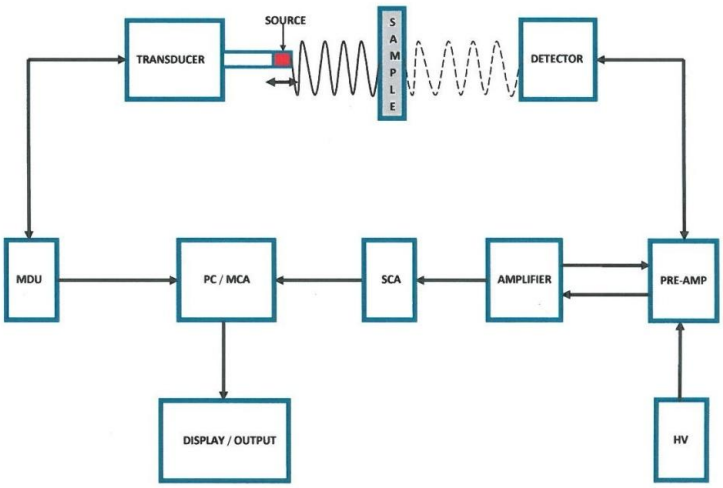

Figure 1. Mössbauer Spectroscopy Block Diagram.

The Mössbauer spectroscopy used for me asurements in the current work consist of an MR-351 Mössbauer drive unit (MDU), a CANBERRA amplifier, IIFAST ComTec pre-amplifier, 5 KV BIN power supply model 1000, an LND INC 45431 nuclear radiation detector and an ORTEC MCS-pciTM data card with multichannel analyser (MCS) software version: 2.13 installed in a desktop computer. A block diagram of the Mössbauer spectrometer is shown in Figure 1. A 25 mCi ^{57}Co source sealed in Rh matrix was attached to the transducer and shielded with about 1 cm thick lead block. The Mössbauer spectrometer was calibrated using an iron foil at room temperature. The MDU provides the mode of vibration of the transducer at constant acceleration to achieve resonant absorption. A sample of about 0.2 g was placed in a plastic sample holder and positioned in the sample space. The transmitted γ ray intensity corresponding to the 14.4 keV interacts with the nucleus of the sample and the transmitted rays through the sample are detected by the detector. These signals are amplified with amplifiers at high voltage (HV) and sent through a single channel analyser (SCA) which is further processed by the multi-channel analyser (MCA) for data capturing by the computer. The accumulated data are interpreted as spectra and displayed on the output screen of the computer using MCS software. A minimum of 15 hours was allowed for data

UNDER PEER REVIEW

accumulation so as to generate good spectra for analysis. The spectra were fitted using recoil Mössbauer analysis software.

3. RESULTS AND DISCUSSION

This section provides details on results and analysis of the magnetic nano ferrites material based on the structural studies, morphological and magnetization measurement.

3.1 X-ray diffraction

The X-ray powder diffraction patterns for $CoFe_2O_4$ and $ZnFe_2O_4$nano-ferrites are shown in Figures 2 and 3. The XRD instrument used in the current work was equipped with a diffracted beam monochromator in the receiving optics equipped with a Cobalt anode at wavelengths λ_1=1.7892 Å, and λ_2=1.7931 Å. The calculated average wavelength λ was 1.7903 Å. The data were collected in a 2θ-range of 10° to 80° at an angular resolution of 0.02°. The results show that no impurity phases are detected in the nano-ferrites samples. All the peaks are indexed with respect to the spinel structure (Joint Committee on Powder Diffraction Standards (JCPDS No. 022-1086) associated with the space group Fd3m [19]. The prominent 311 peak associated with spinel structure can be clearly seen. The broadness of the peaks, especially for the $CoFe_2O_4$ nano-ferrites is indicative of the nano-particle nature of the sample. Therefore, the expectation is that the crystallite size of the $CoFe_2O_4$ nano-ferrites should be smaller compared to that of $ZnFe_2O_4$ nano-ferrites.

The crystal structure analysis were performed using the 311 peak to determine parameters such as the crystallite size *D* and the lattice parameters *a*. The *D* and *a*were calculated using equations 3 and 4, and the obtained values are presented in Table 3.0. As expected from the broadness of $ZnFe_2O_4$nano-ferrites XRD peaks, the crystallite size of the $ZnFe_2O_4$nano-particles is bigger by about 8 nm compared to $CoFe_2O_4$nano-ferrites. This might not be unconnected to the ionic radii of Co and Zn, which are 125 pm and 137 pm respectively [20]. This implies that Zn with larger ionic radius could lead to expansion of the unit cell of $ZnFe_2O_4$nano-ferrites. The values of the lattice parameters, *a,* are consistent with reported values for ferrite spinel structure. No significant increase was, however, observed for *a* in both samples.

UNDER PEER REVIEW

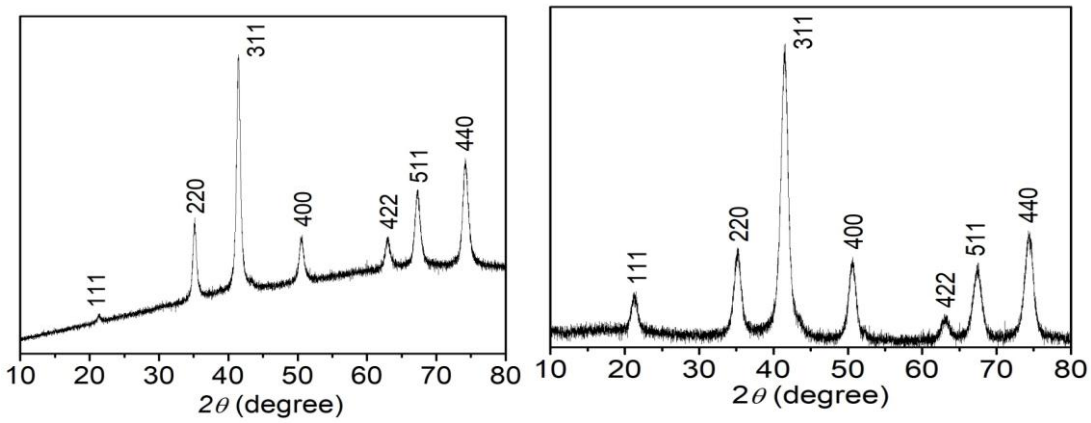

(a) $ZnFe_2O_4$ Ferrites **(b) $CoFe_2O_4$ Ferrites**

Figure 2. X-ray Diffraction patterns for (a) $ZnFe_2O_4$ Ferrites and (b) $CoFe_2O_4$ Ferrites

Table 1. Crystal Structure Parameters, Size (D), lattice parameter (a) for $CoFe_2O_4$ and $ZnFe_2O_4$ Nano-Ferrites

Sample	*D* (nm)±0.24	*a* (Å)±0.005	R^2
$CoFe_2O_4$	10.04	8.384	0.9869
$ZnFe_2O_4$	17.82	8.386	0.9871

3.2 Morphological Studies

The shape of the nano-particles and their surface were examined using high resolution transmission and scanning electron microscopy (HRTEM and HRSEM) respectively. The morphologies of the samples are shown in Figures 2 and 3. The nano-ferrites sample of $CoFe_2O_4$ shows a better crystalline structure with particles of almost spherical shape compared to $ZnFe_2O_4$nano-ferrites. The HRSEM images of both nano-ferrites measured at the same magnification of 100 nm reveal that the particle sizes of the $ZnFe_2O_4$nano-ferrites are bigger than that of $CoFe_2O_4$nano-ferrites. This supports the

UNDER PEER REVIEW

crystallite size estimation from the XRD data. The surface images also show the fairly spherical nature of the nano-particles.

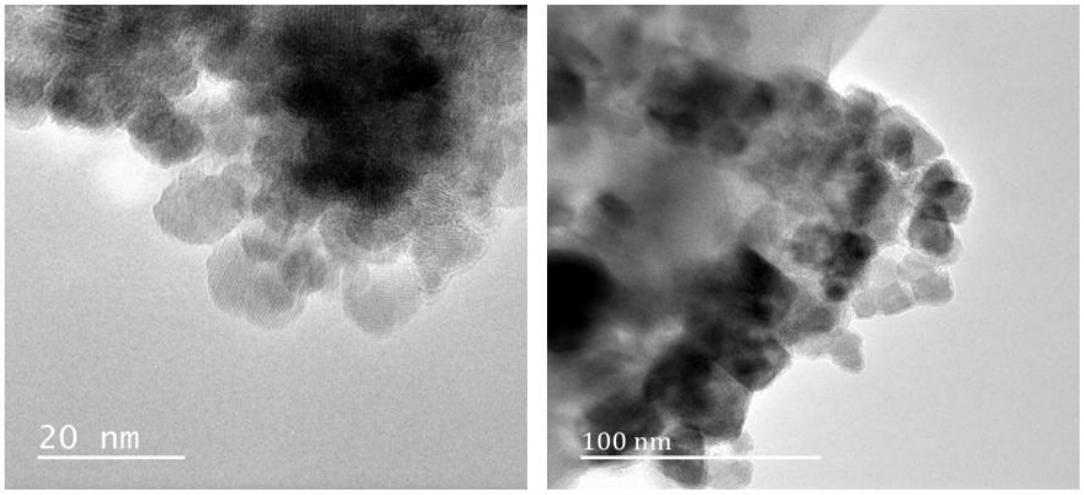

(a) HRTEM image of $CoFe_2O_4$ Nano-Ferrites (b) HRTEM image of $ZnFe_2O_4$ Nano-Ferrites

Figure 3. HRTEM image of Nano-Ferrites Synthesized by Glycol-Thermal Method

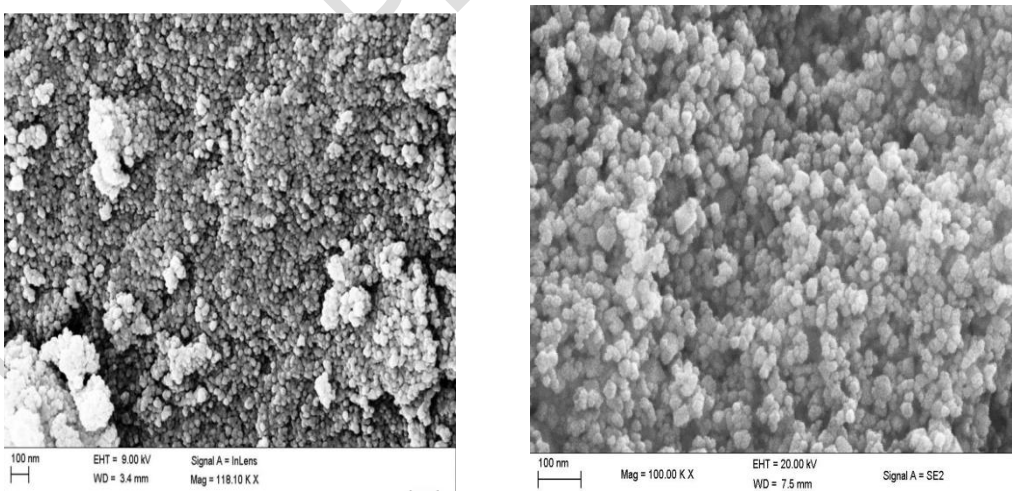

(a) HRSEM image of $CoFe_2O_4$ Nano-Ferrites (b) HRSEM image of $ZnFe_2O_4$ Nano-Ferrites

Figure 4. HRSEM image of Nano-Ferrites Synthesized by Glycol-Thermal Method

3.3 Magnetization Measurements

Magnetization measurements at room temperature were performed on the nano-ferrites samples, using LakeShore model 735 VSM equipment. The magnetic properties such as coercivity H_C and saturation magnetizat sizes as already shown in the VSM results. Similar magnetization results for $CoFe_2O_4$ have been reported by Xing-Hua *et. al.* [22] M_S were estimated from magnetic hysteresis loops. The H_C and M_S were estimated based on Equations 2 and Equation 1 respectively. The magnetic hysteresis loop for $CoFe_2O_4$ nano-ferrites is presented in Figure 4 (a). The fit is shown in Figure 4(b). The hysteresis loop show evidence of superparamagnetic behavior associated with smaller particle. The nano-ferrite had coercivity H_C of about 0.03 kOe and saturation magnetization M_S of about 50 emu/g. These features are desirous for practical application of nano-particles for oil spill cleanup. The implication is that a small magnet will be sufficient to magnetize and demagnetize the sample without significant remnant or residual magnetization in the sample. It also implies that during the recycling process of the nano-particles, magnet with little magnetic field strength can help perform the cycle of magnetization with swift response to the magnetic field.

PEER REVIEW

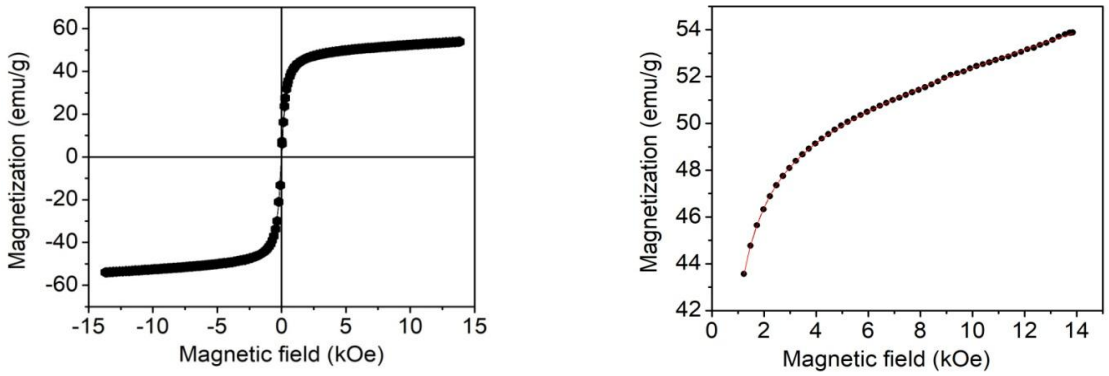

Figure 5. (a) Room Temperature hysteresis loops of $CoFe_2O_4$nano-ferrites, (b) A fit Approach to Saturation Magnetization of the High Field initial Magnetization of $CoFe_2O_4$ (Equation 1).

Similar analysis was performed on the $ZnFe_2O_4$ nano-ferrites particles. The hysteresis loop is presented in Figure 5(a). The magnetic loop appears to show mixed magnetic phases of super-paramagnetism and paramagnetism. The paramagnetic component can be observed from the steep shape of the hysteresis loop. Coercivity, H_C, of about 0.20 kOe and saturation magnetization M_S of about 30 emu/g were obtained. The low magnetization value when compare to that obtained for $CoFe_2O_4$ nano-ferrites could be attributed to unpaired electrons in the valence shell of Zn atoms, thereby causing a poor magnetic response of the $ZnFe_2O_4$ nano-ferrites. Thus could also explain why there is a slight increase in the coercivity because, non-magnetic atoms within a cluster of magnetic spins could increase coercivity [23]. Although, $CoFe_2O_4$ nano-ferrites showed the most desirous properties for application, $ZnFe_2O_4$ nano-ferrites is less toxic. Therefore, its response to the application and removal of magnetic field could be slow, it will be environmentally friendly.

The obtained parameters from the fit to the law of approach to saturation magnetization of Equation 1 are presented in Figure 5(b). The significant change in the a parameter for $ZnFe_2O_4$nano-ferrites is indicative of a nonmagnetic inclusions arising from Zn atoms.

UNDER PEER REVIEW

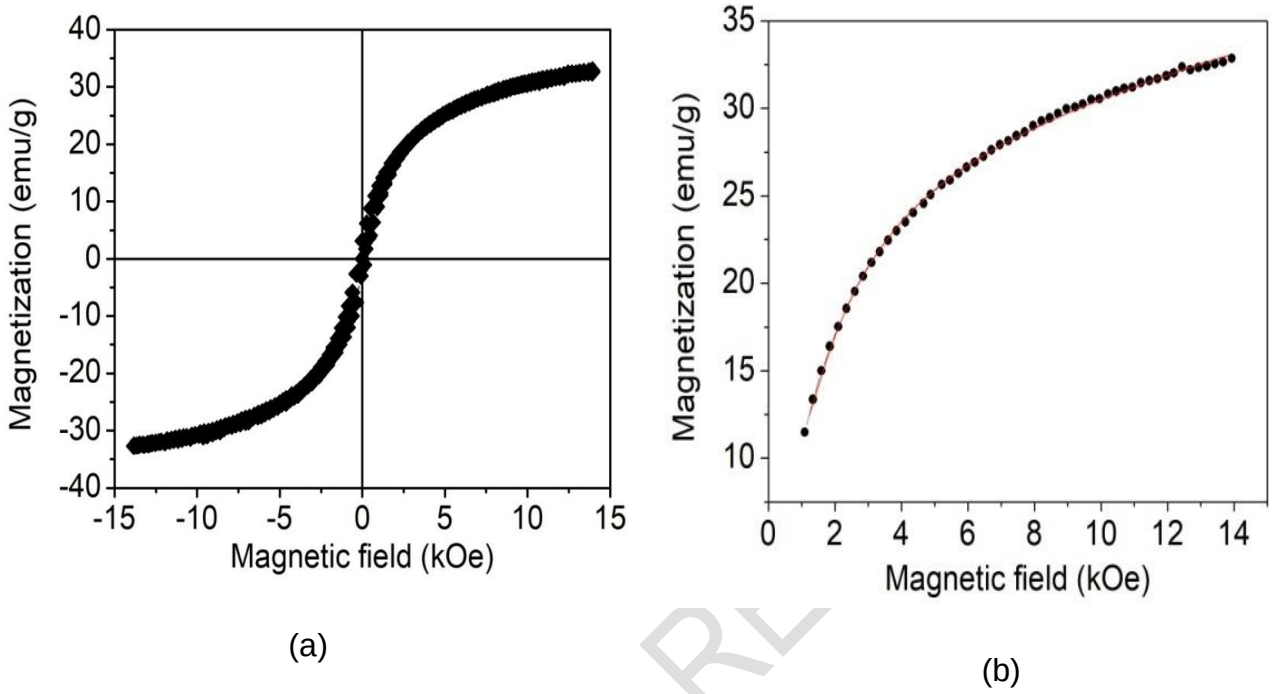

Figure 6. (a) Room Temperature hysteresis loops of $ZnFe_2O_4$nano-ferrites, (b) A fit Approach to Saturation Magnetization of the High Field initial Magnetization of $ZnFe_2O_4$ (Equation 1).

3.4 ^{57}Fe Mössbauer Spectroscopy Measurements

The ^{57}Fe Mössbauer spectroscopy measurements for the $CoFe_2O_4$ and $ZnFe_2O_4$ nano-ferrites were performed at room temperature. The calibration was done using α-Fe foil at a constant acceleration. The magnetic components of the spectra were fitted using the Lorentzian site analysis in Recoil Mössbauer analysis software.

Two sextets' δ_1 and δ_2, were best suited to model the $CoFe_2O_4$ nano-ferrites as shown in Figure 6. The spectra shows a well ordered magnetic phase where sextets' δ_1 and δ_2 are associated with Fe^{3+} ions at tetrahedral A-sites and octahedral B-sites of the spinel crystal structure [24]. Table 2 gives the values of the magnetic hyperfine field, H_{Bf}, isomer shift, *IS*, quadrupole splitting, Δ_{EQ}, and the fraction population, *f*, of Fe^{3+} ions. The higher field of about 482 kOe is attributed to the B-sites and the lower field of about 445 kOe associated with the A-sites. The isomer shift values are in the appropriate range for Fe^{3+} [25] and the

UNDER PEER RE

hyperfine magnetic field are close to reported values [26]. Therefore, no evidence of Fe^{2+} is observed.

Table 2. Mössbauer parameters obtained from fit, where H_{bf} is the hyperfine magnetic field, isomer shifts (*IS*), quadrupole splitting (Δ_{EQ}), fraction populations (*f*) and reduced chi^2 (c^2) of Fe ions of $CoFe_2O_4$nano-ferrites samples

Sample	Sites	H_{Bf}(kOe)	δ (mm/s)	Δ_{EQ} (mm/s)	*f* (%)	c^2
		±1.3	±0.02	±0.00	±2	1.3110
$CoFe_2O_4$	δ1 (A-site)	445.3	0.31	0.01	30	
	δ2 (B-site)	482.3	0.31	0.01	70	

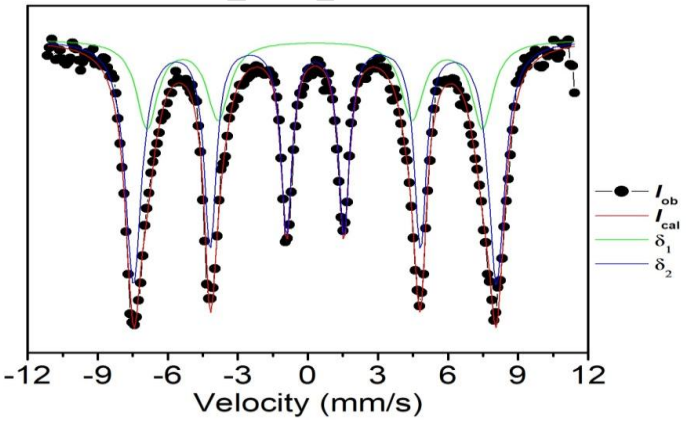

Figure 7. Fit to ^{57}Fe Mössbauer Spectra for $CoFe_2O_4$ Nano-Ferrites.

However, the $ZnFe_2O_4$ nano-ferrite was not a well ordered sextet compared to $CoFe_2O_4$ nano-ferrite, and it was best fitted with two sextets and two doublets as shown in Figure 7. The results are shown in Table 3. The effect of the paramagnetic component can be seen to have a dropping effect and broadness of the spectra. The two sextets are associated with the coordination of Fe^{3+}ions at tetrahedral A and octahedral B sites of the

UNDER PEER REVIEW

spinel crystal structure [27]. The doublets account for the paramagnetic component as was observed in the magnetic hysteresis loops. Again, the isomer shift values are in the appropriate range for Fe^{3+}. Higher values of quadrupole splitting indicate that the ions are imbedded in non-cubic surroundings, while the relatively small values of the quadrupole splitting indicate that A and B sites have nearly cubic symmetry.

Table 3. Mössbauer parameters obtained from fit, where H_{bf} is the hyperfine magnetic field, isomer shifts (*IS*), quadrupole splitting (Δ_{EQ}), fraction populations (*f*) and reduced chi^2 (c^2) of Fe ions of $ZnFe_2O_4$nano-ferrites samples.

Sample	Sites	H_{Bf}(kOe)	δ (mm/s)	Δ_{EQ} (mm/s)	*f* (%)	c^2
		±1.2	±0.02	±0.00	±1	
$ZnFe_2O_4$	δ1 (A-site)	408	0.32	0.00	24	1.1102
	δ2 (B-site)	470	0.31	-0.00	15	
	D_1		0.37	7.22	30	
	D_2		0.35	1.03	32	

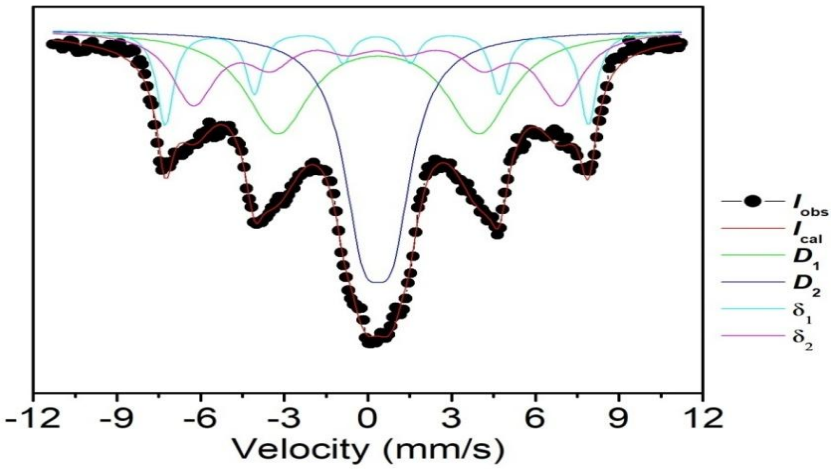

Figure 8. Fit to ^{57}Fe Mössbauer spectra for $ZnFe_2O_4$nano-ferrites

UNDER PEER REVIEW

4. CONCLUSIONS

Magnetic nano-particles possess the potential to be used for environmental remediation. Certain magnetic properties are expected for such application. This work studied the structural and magnetic properties of $CoFe_2O_4$ and $ZnFe_2O_4$nano-ferrites synthesized by glycol-thermal technique. The properties that support their application for oil spill cleanup are considered. Structural properties were investigated by X-ray diffraction technique from which information such as crystallite size and lattice parameters were determined. The $CoFe_2O_4$ and $ZnFe_2O_4$nano-ferrites samples were single phase cubic spinel structure without any impurity phase. Larger crystallite size of about 17 nm was obtained for $ZnFe_2O_4$nano-ferrites compared to about 10 nm obtained for $CoFe_2O_4$nano-ferrites. Such large size was attributed to lager atomic radii of Zn atoms. No significant changes occurred in the lattice parameters. The high resolution transmission electron microscopy and surface microscopy showed that nano structure and the almost-spherical shape of the nanoparticles.

Room temperature magnetization results of the two samples show evidence of superparamagnetic behavior for $CoFe_2O_4$nano-ferrites. However, a mixed magnetic phase of superparamagnetism and paramagnetism appear to be the case for $ZnFe_2O_4$ nano-ferrites. $CoFe_2O_4$ has a low coercivity and high magnetization compared to $ZnFe_2O_4$ nano-ferrites. This suggests that the nanoparticles will respond to small magnetic field when such particles are used for environmental remediation such as oil spill cleanup. However, it has a disadvantage of toxicity at high concentration dosage compared to $ZnFe_2O_4$ nano-ferrites that is environmentally friendly. Hence, $ZnFe_2O_4$ nano-ferrites might have a slow response to magnetic field, it possess higher potential for environmental sustainable when considering the two samples studied in this work. The room temperature ^{57}Fe Mössbauer spectra show ordered magnetic structures for $CoFe_2O_4$ that were resolved with two sextets. The internal magnetic field splitting and isomer shifts values are consistent with that of ferrites. The evidence of paramagnetic component in $ZnFe_2O_4$ nano-ferrites was further revealed by the ^{57}Fe Mössbauer measurements. Two sextets and two doublets were used to resolve the

UNDER PEER REVIEW

spectra. Isomer shifts on A-, B- and doublet sites are consistent with Fe^{3+} ions. No evidence of other oxidation state of Fe was seen. The hyperfine fields based on the Lorentzian site analysis for $ZnFe_2O_4$ nano-ferrites were lower compared to $CoFe_2O_4$ nano-ferrites. The glycol-thermal synthesis method is a viable method to produce nano-ferrites with single phase.

From the single phase of $CoFe_2O_4$ nano-ferrites and $ZnFe_2O_4$ nano-ferrites which ware synthesized by glycol-thermal method at 200 ºC we are able to show from ^{57}Fe Mössbauer spectroscopy measurement that the oxidation state of Fe was stable at Fe^{3+} such stability in the oxidation state of Fe helps in reusability of the nanoparticles after every cycle of clean up. This is important because the magnetic properties of the nanoparticles can be fairly predicted not change significantly to affect its application around room temperature. We are also able to find that $CoFe_2O_4$has a low desirable coercivity property making it a better candidate for possible oil spill cleanup compared to the $ZnFe_2O_4$studied in the current work.

COMPETING INTERESTS DISCLAIMER:

Authors have declared that no competing interests exist. The products used for this research are commonly and predominantly use products in our area of research and country. There is absolutely no conflict of interest between the authors and producers of the products because we do not intend to use these products as an avenue for any litigation but for the advancement of knowledge. Also, the research was not funded by the producing company rather it was funded by personal efforts of the authors.

UNDER PEER REVIEW

REFERENCES

1. Kirubakaran, Sivapriya, and Vijay Thiruvenkatam. "Diverse Applications of Nanotechnology in Biomedicine, Chemistry, and Engineering." In

Handbook of Research on Diverse Applications of Nanotechnology in Biomedicine, Chemistry, and Engineering, IGI Global (2015): 1-9.

2. Khalil, Munawar, Badrul Mohamed Jan, Chong Wen Tong, and Mohammed Ali Berawi. "Advanced nanomaterials in oil and gas industry: design, application and challenges." *Applied energy* 191 (2017): 287-310.

3. Ko, Saebom, Eun Song Kim, Siman Park, Hugh Daigle, Thomas E. Milner, Chun Huh, Martin V. Bennetzen, and Giuliano A. Geremia. "Amine functionalized magnetic nanoparticles for removal of oil droplets from produced water and accelerated magnetic separation."*Journal of Nanoparticle Research* 19, no. 4 (2017): 132.

4. Fakoya, MuiliFeyisitan, and SubhashNandlal Shah. "Emergence of nanotechnology in the oil and gas industry: Emphasis on the application of silica nanoparticles." *Petroleum* 3, no. 4 (2017): 391-405.

5. El-Diasty, Abdelrahman Ibrahim, and Adel M. Salem Ra.lo00gab. "Applications of nanotechnology in the oil & gas industry: Latest trends worldwide & future challenges in Egypt." In *North Africa Technical Conference and Exhibition*. Society of Petroleum Engineers, 2013.

6. Valenzuela, F. J., A. Perez-Sepulveda, M. J. Torres, and P. Correa. "Re petto GM, Illanes SE." *Pathogenesis of preeclampsia: the genetic component. J Pregnancy* 2012 (2012): 632732.

7. Pandey, Brajesh, F. J. Litterst, and E. M. Baggio-Saitovitch. "Preferential spin canting in nanosize zinc ferrite." *Journal of Magnetism and Magnetic Materials* 385 (2015): 412-417

8. Hill, Patricia M., H. S. Peiser, and J. R. Rait. "The crystal structure of calcium ferrite and β calcium chromite." *ActaCrystallographica* 9, no. 12 (1956): 981-986.

UNDER PEER REVIEW

9. Ramarao, Rajesh Babu, Kishore Babu, Veeraiah, Ramarao, Rajasekhar, and Venkateswara Rao "Influence of Zn Substitution on Structural, Magnetic and Electrical Properties of MgFe2O4" *Journal of Electronic Materials* (2018): ISSN 0361-5235

10. Msomi, J.Z., Dlamini, W.B., Moyo, T. and Ezekiel, P. "Investigation of phase formation of (Zn, Mg)$_{0.5}$Co$_{0.5}$Fe$_2$O$_4$nanoferrites". *Journal of Magnetism and Magnetic Materials*, 373, (2015): pp.68-73.

11. Andreev, S. V., M. I. Bartashevich, V. I. Pushkarsky, V. N. Maltsev, L. A. Pamyatnykh, E. N. Tarasov, N. V. Kudrevatykh, and T. Goto. "Law of approach to saturation in highly anisotropic ferromagnets Application to Nd-Fe-B melt-spun ribbons." *Journal of alloys and compounds* 260, no. 1-2 (1997): 196-200.

12. Guo, X., X. Chen, Z. Altounian, and J. O. Ström-Olsen. "Temperature dependence of coercivity in MnBi." *Journal of applied physics* 73, no. 10 (1993): 6275-6277.

13. Simonsen, Galina, Mikael Strand, and Gisleøye. "Potential applications of magnetic nanoparticles within separation in the petroleum industry." *Journal of Petroleum Science and Engineering* (2018).

14. Kodama, R.H. "Magnetic nanoparticles". *Journal of magnetism and magnetic materials*, 200 no. 1-3 (1999): 359-372.

15. Rocco, D. L., A. A. Coelho, S. Gama, and M. de C. Santos. "Dependence of the magnetocaloric effect on the A-site ionic radius in isoelectronic manganites." *Journal of Applied Physics* 113, no. 11 (2013): 113907

16. Rostamnejadi, A., M. Venkatesan, P. Kameli, H. Salamati, and J. M. D. Coey. "Magnetocaloric effect in La$_{0.67}$Sr$_{0.33}$MnO$_3$ manganite above room temperature." *Journal of Magnetism and Magnetic Materials* 323, no. 16 (2011): 2214-2218

UNDER PEER REVIEW

17. Kittel, Charles, Paul McEuen, and Paul McEuen. Introduction to solid state physics.
Vol. 8. New York: Wiley, 1996.

18. Cullity D. B., Elements of X-ray Di_raction, 2nd Ed. Addison- Wesley publishing company (1977) 356-102.

19. Park, C. H., Na, J. G., Heo, N. H., Lee, S. R., Kim, J., & Park, K. (1998). Characterization of Metal/Cobalt Ferrite Magnetic Thin Films. *Journal of Magnetics*, *3*(1), 31-35

20. Wells, A. F. (1984). The lanthanides and actinides. In *Structural inorganic chemistry. 5. ed*. 1288.

21. Li, X. H., Xu, C. L., Han, X. H., Qiao, L., Wang, T., & Li, F. S. (2010). Synthesis and magnetic properties of nearly monodisperse CoFe 2 O 4 nanoparticles through a simple hydrothermal condition. *Nanoscale research letters*, *5*(6), 1039-1044.

22. Li, Qing, Christina W. Kartikowati, Shinji Horie, Takashi Ogi, Toru Iwaki, and KikuoOkuyama. "Correlation between particle size/domain structure and magnetic properties of highly crystalline Fe_3O_4 nanoparticles." *Scientific reports* 7, no. 1 (2017): 1-7.

23. Bauer, J., & Seeger, M. (1996). Zern A and Kronmüller H. *J. Appl. Phys.*, *1996*, 80.

24. Gismelseed, A. M., Mohammed, K. A., Widatallah, H. M., Al-Rawas, A. D., Elzain, M. E., &Yousif, A. A. (2010, March). Structure and magnetic properties of the $Zn_xMg_{1-x}Fe_2O_4$ ferrites. In *Journal of Physics: Conference Series* (Vol. 217, No. 1, p. 012138). IOP Publishing.

25. Rao, B. P., Rao, P. S., Murthy, G. V. S., & Rao, K. H. (2004). Mössbauer study of the system $Ni_{0.65}Zn_{0.35}Fe_{2-x}Sc_xO_4$. *Journal of magnetism and magnetic materials*, *268*(3), 315-320.

26. Johnson, C. E., Ridout, M. S., &Cranshaw, T. E. (1963). The Mössbauer effect in iron alloys. *Proceedings of the Physical Society (1958-1967)*, *81*(6), 1079.

UNDER PEER REVIEW

27. Pankhurst, Q. A., & Pollard, R. J. (1991). Origin of the spin-canting anomaly in small ferrimagnetic particles. *Physical review letters*, *67*(2), 248.

UNDER PEER REVIEW